THE JOURNAL OF PHYSICAL CHEMISTRY B

ARTICLE

pubs.acs.org/JPCB

Modeling Thermal Decomposition Mechanisms in Gaseous and Crystalline Molecular Materials: Application to β-HMX

Onise Sharia and Maija M. Kuklja*

Department of Materials Science and Engineering, University of Maryland, College Park, Maryland 20742, United States

ABSTRACT: Exploration of initiation of chemistry in materials is especially challenging when several coexisting chemical mechanisms are possible and many reactions' products are produced. It is even more difficult for complex materials, such as molecular, supramolecular, and hierarchical materials and systems. A strategy to draw a complete picture of the earliest stages of rapid decomposition reactions in molecular materials is presented in this study. The strategy is based on theoretical and computational modeling of chemical decomposition reactions in the gaseous and crystalline molecular material that has been performed by means of combined density functional theory and transition state theory. This study reveals how a crystalline field affects materials chemical degradation. We also demonstrate how incomplete results, which are often used due to difficulties in obtaining comprehensive data, can lead to erroneous conclusions and predictions. We discuss our approach in the context of the obtained reaction energies, activation barriers, structures of transition states, and reaction rates with the example of a representative molecular material, β-HMX, which tends to decompose violently with large energy release upon an external perturbation. The performed analysis helps to provide a consistent interpretation of available experimental data. The article illustrates that the complete picture of decomposition reactions of complex molecular materials, while theoretically challenging and computationally demanding, is possible and even practical at this point in time.

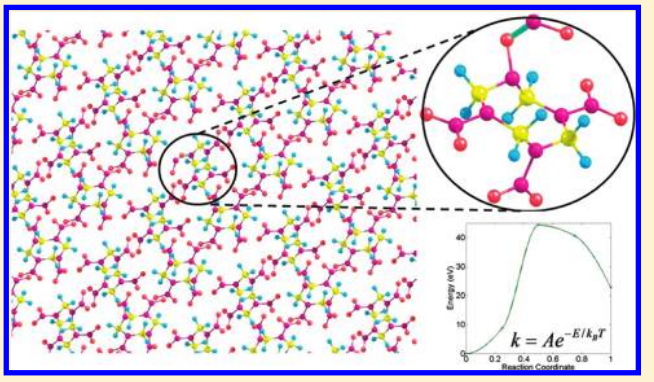

I. INTRODUCTION

Molecular materials offer a broad range of existing and potential applications, going from molecular electronics and single molecule devices to nanotechnology and data storage to sensors, detectors, and energy conversion mechanisms. Basic research into the optical, electronic, and magnetic properties of molecular materials is thriving and has led to, among other inventions, a new generation of electronic devices and displays. The proper physical description of such materials remains a challenge, as it includes aspects of condensed matter physics, solid state and molecular chemistry, and materials science all at once. This article presents a point of view on thermal decomposition processes and kinetics of molecular materials starting from single molecules going to single crystals, and merges several theories and methods. The objective of the research is to investigate and develop a first-principles fundamental and holistic understanding of the decomposition process of complex functional molecules and crystalline materials built of said molecules. Upon gaining this understanding, we may find ways of designing new materials with tailored properties or developing strategies for tuning properties of existing materials. The interest for stability of these functional molecular materials is motivated by the scientific challenge they pose to physics and chemistry of fast chemical reactions coupled with the intriguing complexity of their crystalline arrangements and internal interactions.

For the theoretical comparative analysis of the thermodecomposition process of a gaseous and crystalline molecular material, we selected an illustrative example of β-octahydro-1,3,5,7-tetranitro-1,3,5,7-tetrazocine (β-HMX). We think it serves as an ideal model system for the task. β-HMX is an important energetic material for many technological applications,[1] which decomposes violently with large energy release upon an external stimuli.[2−4] One of the challenging issues is to understand its dissociation reactions at the very initial stage of detonation in order to control the material's behavior and optimize its safe handling and use. For the time being, this is a very difficult, dangerous, and nearly impossible task from an experimental point of view alone.

Our knowledge of the condensed phase chemistry in molecular materials, including HMX, is limited to global reaction kinetics and final products that we usually interpret in an attempt to reproduce the net reactions of the decomposition process.[4−8] Our interpretations are most often based on speculations because elementary reaction steps in condensed phase energetic materials are not universally established and are especially difficult to tackle experimentally when several parallel reactions occur.

Received: March 23, 2011
Revised: September 21, 2011
Published: September 26, 2011

Although properties of HMX have been, and are being extensively studied experimentally in solid, melt, and gas phases (see, for example, refs 5 and 7−11), elucidation of the initial steps in the decomposition process of energetic solids is particularly difficult and remains a significant challenge.[6−8,12] The thermal decomposition of HMX is believed to involve many chemical species and hundreds of elementary reactions[12−14] and includes a $\beta \rightarrow \delta$ phase transition at 165−210 °C.[8,15−18] There is very limited research carried out at the level of *ab initio* theoretical methods,[19,20] with most theoretical work performed on gas phase molecules.[21,22] Among possible initial decomposition reactions of nitramines are the N−NO_2 bond fission,[6,23−27] the HONO elimination,[6,25,26] and the nitro-nitrite isomerization.[6,28] Some other mechanisms, such as various ways of breaking the molecular ring, were also proposed. It is not firmly determined which of these is dominant for any of the nitramines, even in the gas phase.[6,8,29,30] Most experimental and theoretical studies indicate that the N−NO_2 bond fission has the lowest-energy barrier; however, the reported computed and experimental values of the reaction barriers and the associated kinetic parameters for various nitramines under various conditions show a fair amount of dispersion (see, for example, refs 6, 11, 27, 29, and 30 and references therein).

We performed a combined study based on density functional theory calculations coupled with the conventional transition state theory (CTST)[31] and variational transition state theory (VTST)[32] to analyze the effect of the crystalline field on the interplay of main decomposition reactions in HMX. Our conclusions are based on the obtained activation barriers of chemical reactions, structures of transition states, pre-exponential factors, and reaction rates, which are required to draw a complete picture of the earliest stages of the decomposition process. In this article, we focus on perfect crystals; however, defects and deformations can also be considered.[33] We believe that this strategy is applicable to any molecular material and can be extended to supramolecular and hierarchical materials as well.

First, we discuss and simulate six probable mechanisms for detonation initiation in the HMX gas phase. Then, we select only three of these reactions, the N−NO_2 cleavage, the intramolecular hydrogen transfer leading to the HONO elimination, and the nitro-nitrite isomerization (or NONO rearrangement), which have relatively low activation barriers and relatively high reaction rates, and extend our calculations to the solid phase. We comment on the revealed differences between solid and gas phase decompositions that prove that the crystalline field affects both activation barriers and reaction rates and, hence, the bond-breaking processes in molecules and molecular materials are strongly dependent upon the molecular environment. We analyze our results in the context of available experimental data and provide specific recommendations for modeling of practical molecular crystal samples.

II. THEORETICAL METHODS

In calculations, we use the plane wave density functional theory[34,35] in the GGA approximation with the PBE functional[36] and PAW[37] method as implemented in VASP codes.[38−40] The kinetic energy cutoff is set to 600 eV. For the HMX unit cell of 6.7 × 11.4 × 8.9 Å^3 size, we use a 2 × 2 × 2 Monkhorst−Pack[41] k-point mesh. For larger cells, we reduce the number of k-points accordingly. Atomic positions are relaxed using the conjugate gradient and quasi-Newton methods within a force tolerance of 0.05 Å/eV.

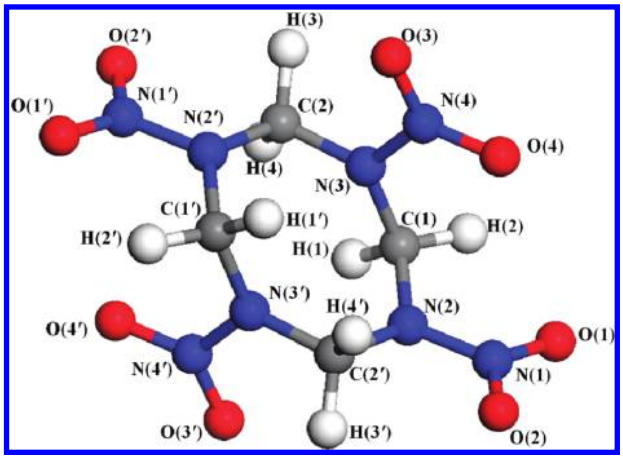

Figure 1. The atomistic structure of an HMX molecule in the crystalline β-phase.

Table 1. Comparison of Theoretical and Experimental Lattice Constants of HMX

	theoretical (this study)	experimental (ref 43)	other theory (ref 44)	error (%)
a	6.72 Å	6.54 Å	6.52 Å	2.9
b	11.41 Å	11.05 Å	10.99 Å	3.2
c	8.91 Å	8.70 Å	8.62 Å	2.3
β	124.06°	124.3°	122.73°	0.2

The β-phase, the most stable HMX structure under ambient conditions, has a monoclinic structure with $P2_1/c$ ($P2_1/n$) symmetry and two molecules per unit cell[42,43] (Figure 1). There are two types of nitro groups in each molecule, the axial (O(1)−N(1)−O(2)) and the equatorial (O(3)−N(4)−O(4)). The eight-member ring in the β-HMX molecule has a chair configuration, with the two equatorial (and axial) NO_2 groups attached on the opposite sides of the ring plane (C(1)−C(2)−C(1′)−C(2′) plane). The quality of the calculations for the ideal crystal is illustrated with the optimized geometry that was obtained by relaxing both lattice constants and atomic positions. We compare the theoretical lattice constants with the results of earlier work[44] and experimental data[43] in Table 1. The parameters of the theoretical crystalline structure are 0−3% larger than experimental ones, which is within a typical GGA accuracy. The molecular geometry, the bond lengths and bond angles, summarized in Tables 2 and 3, are in good agreement with experimental values.

To find the minimal energy path of each reaction and the corresponding transition state, we use the climbing nudged elastic band method (CNEBM)[45] with six intermediate images between the initial and final atomic configurations. Reaction energy is defined as the difference between the total energies of the initial and final states of the system. Barrier activation energy is determined as the difference between the total energies of the initial and transition states. Details of the reaction rate calculations are described in the next section.

III. DECOMPOSITION MECHANISMS

Following a general theory of chemical reactions,[46] the dependence of a reaction rate on temperature T can be described

Table 2. Bond Lengths for Bulk β-HMX (For the Notations of Atoms, Refer to Figure 1)

bond	bond length (Å) (this study)	bond length (Å) (Exp., ref 43)	error (%)
N(2)−C(1)	1.454	1.448	0.4
N(2)−C(2′)	1.484	1.471	0.8
N(3)−C(1)	1.459	1.455	0.3
N(3)−C(2)	1.439	1.437	0.1
N(2)−N(1)	1.373	1.354	1.4
N(3)−N(4)	1.391	1.373	1.3
N(1)−O(1)	1.240	1.233	0.6
N(1)−O(2)	1.249	1.222	2.2
N(4)−O(3)	1.237	1.210	2.3
N(4)−O(4)	1.240	1.204	3.0
C(1)−H(1)	1.098	1.111	1.1
C(1)−H(2)	1.095	1.091	0.4
C(2)−H(3)	1.096	1.101	0.4
C(2)−H(4)	1.097	1.095	0.2

by the Arrhenius equation and characterized by a pre-exponential factor A and an activation barrier E:

$$k = Ae^{-E/k_BT} \quad (1)$$

k_B is the Boltzmann constant. In our study, we first calculate activation barriers for several candidate reactions. The reactions that exhibit a high activation energy, 15 kcal/mol higher than the lowest reaction, will be considered as unfavorable mechanisms, because their rates are small due to the dominating exponent contribution regardless of the value of the Arrhenius factor. For all low energy reactions, we calculate pre-exponential factors and then compare their rates. In our modeling, all calculations are performed at zero pressure.[47]

III.1. Gas Phase HMX Molecule. In order to model an isolated molecule, we constructed a 15 × 15 × 15 Å^3 cell containing a single β-HMX molecule. The size of the periodic cell ensures that spurious interactions between molecules from the translated cells are negligible. Calculations were performed only at the Gamma point of the Brillouin zone. In the initial guess, the structure of the molecule was taken from the bulk β-HMX crystal, which was then allowed to relax by minimizing the total energy. The relaxation energy was found to be relatively small, 1.44 kcal/mol, and the atomic positions did not significantly change during the relaxation. Next, we consider several dissociation mechanisms of this molecule.

HONO Elimination. The HONO elimination is often suggested as a low energy first decomposition step in nitramines.[6,7,11,26] The reaction is believed to proceed in two steps. A HONO isomer forms first due to the hydrogen transfer, and then the entire HONO moiety splits off of the parent molecule. To simulate a HONO isomer[48] in calculations, we transfer an H atom to the closest NO_2 group within the same molecule. For the equatorial NO_2 (O(3)−N(4)−O(4)), we remove the H(3′) atom and attach it to the O(3′) atom (referred to hereafter as e-HONO in Figure 2a), and for the axial nitro group (O(1)−N(1)−O(2)), we attach the H(3′) to the O2 (referred to as a-HONO in Figure 2b). In both cases, after the relaxation, the N−N bond breaks spontaneously (no additional energy is required); however, a weak attractive interaction between the HONO and the rest of the molecule continues as the HONO stays in close vicinity to the molecule (Figure 2). The N−N distance in the final state for e-HONO is 3.27 Å and for a-HONO is 3.32 Å. Although the formation energy of the axial

Table 3. Bond Angles for Bulk β-HMX (For the Notations of Atoms, Refer to Figure 1)

bond angle	angle (deg) (this study)	angle (deg) (Exp., ref 43)	error (%)
O(1)−N(1)−N(3)	125.6	126.9	1.0
N(2)−N(1)−O(1)	118.5	118.0	0.4
N(2)−N(1)−O(2)	115.8	116.1	0.3
N(1)−N(2)−C(2′)	115.6	115.2	0.4
N(1)−N(2)−C(1)	118.8	118.8	0.0
C(1)−N(2)−C(2′)	123.2	122.4	0.7
N(2)−C(1)−N(3)	112.4	113.5	1.0
N(2)−C(1)−H(1)	110.7	108.5	2.0
N(2)−C(1)−H(2)	106.9	109.8	2.6
N(3)−C(1)−H(1)	106.6	106.6	0.0
N(3)−C(1)−H(2)	111.5	111.8	0.3
H(1)−C(1)−H(2)	108.7	106.2	2.3
O(3)−N(4)−O(4)	126.6	126.7	0.1
N(3)−N(4)−O(3)	116.9	115.9	0.9
N(3)−N(4)−O(4)	116.5	117.4	0.8
N(4)−N(3)−C(1)	118.4	117.4	0.9
N(4)−N(3)−C(2)	118.2	118.2	0.0
C(1)−N(3)−C(2)	122.8	123.8	0.8
N(2′)−C(2)−N(3)	110.8	110.2	0.5
N(3)−C(2)−H(4)	107.9	107.3	2.7
N(3)−C(2)−H(3)	110.0	110.5	0.5
N(2′)−C(2)−H(4)	110.0	110.1	0.1
N(2′)−C(2)−H(3)	108.7	109.2	0.5
H(3)−C(2)−H(4)	109.4	109.6	0.2

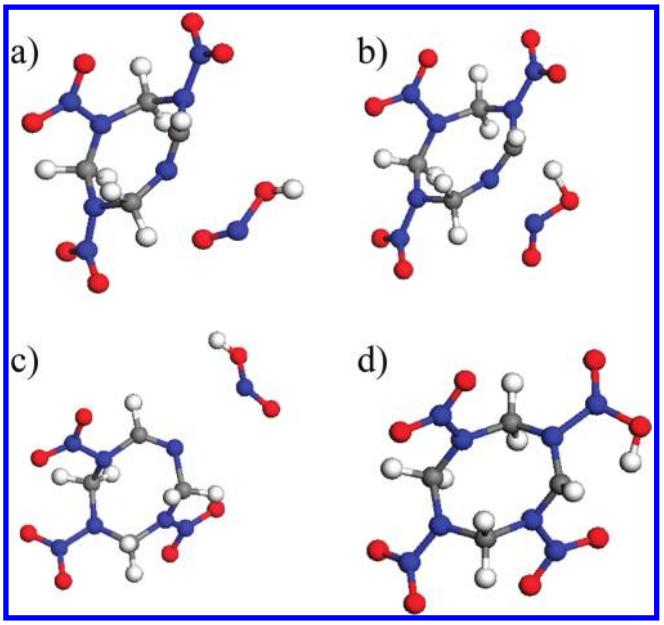

Figure 2. Model configurations used in calculations are shown: (a) the split off equatorial HONO state, (b) e-HONO at the transition state, (c) the split off axial HONO state, and (d) a-HONO at the transition state.

Table 4. Reaction Energies and Activation Barriers for Simulated HMX Decomposition Reactions

reaction	reaction energy (kcal/mol)	activation barrier (kcal/mol)	zero point energy corrected activation barrier (kcal/mol)	log A (s^{-1})
		Gas Phase HMX Molecule Decomposition		
a-HONO elimination	2.34	43.39	39.4	14.23
e-HONO elimination	3.73	44.59		
a-N−NO_2 homolysis (spin nonpolirized)	57.81	57.81	52.3	18.98
e-N−NO_2 homolysis (spin nonpolarized)	56.70	56.70		
a-N−NO_2 homolysis (spin polarized)	42.84	42.84	38.1	17.85
e-N−NO_2 homolysis (spin polarized)	44.62	44.62		
a-NONO formation	22.03	57.09		
e-NONO formation ("outward")	22.89	49.84	45.80	14.85
e-NONO formation ("inward")	22.81	44.39	40.53	15.92
$2C_2H_4N_4O_4$	97.23	97.23		
$CH_2N_2O_2$ + open RDX	69.96	70.19		
$4C_2H_4N_4O_4$	65.50	82.98		
		Bulk Ideal HMX Crystal Decomposition		
a-N−NO_2 homolysis	46.09	47.87	43.67	15.61
a-HONO elimination	13.96	47.93	45.01	14.29
e-HONO elimination	20.50	52.27		
a-NONO rearrangement	29.53	52.74	49.22	14.95
e-NONO rearrangement	32.82	53.92		

HONO isomer (2.34 kcal/mol) is fairly close to the formation energy of the equatorial HONO isomer (3.73 kcal/mol) and their activation barriers are also quite similar (43.39 kcal/mol for axial and 44.59 kcal/mol for equatorial) (Table 4), there is a significant difference between the atomic structures of corresponding transition states, as illustrated in Figure 2. At the transition point of the equatorial nitro group, the N−N bond is broken, while for the axial nitro group the bond still exists. The N−N distances are 2.02 and 1.36 Å for the equatorial and axial nitro groups, respectively. We also calculated vibrational frequencies and found that there is only one negative frequency, which ensures that the true transition state was found in each case. Interestingly, both HONOs (of equatorial and axial nitro groups) split off of the HMX molecule spontaneously right after the formation of the isomer; however, their different N−N bond lengths caused the transition state configurations to be different.

N−NO_2 Homolysis. The dissociation reaction producing a free NO_2 is most supported by experiments as a decomposition initiation mechanism and often is viewed as a rate determining step in the global decomposition kinetics of nitro compounds.[6,26] To simulate N−NO_2 homolysis, we extend the N−N bond until it is broken. First, we tried this using spin nonpolarized DFT calculations.[49] Obviously, the equatorial and axial N−NO_2 bonds behave differently. An elongation of the axial N−N bond to 5.7 Å leads to the bond breaking and splitting off the NO_2, which stays separated from the molecule after the relaxation is complete; this indicates that the axial NO_2 group does not interact with the molecule after the bond fission. The reaction energy of the free NO_2 molecule formation is 57.81 kcal/mol. However, NEBM calculations fall short in finding a barrier in the course of the reaction (Figure 3). Thus, the activation barrier is assumed to be the same as the reaction energy, 57.81 kcal/mol, implying that there is no barrier for the reaction. This is consistent with earlier findings for the decomposition of methylnitramine, a prototype material of nitramines.[7,14] An extension of the equatorial N−NO_2 bond also leads to the bond breaking. However, due to a small attraction between the $C_4H_8N_7O_6$ radical and the NO_2, the structural relaxation causes the NO_2 to rebind with the rest of the molecule. Therefore, in order to determine the activation barrier and reaction energy for the equatorial N−NO_2 bond cleavage process, we fix the N−N distance at 5.2 Å and let the system relax. The calculated formation energy is 56.70 kcal/mol. We note that both energies (57.81 and 56.70 kcal/mol) obtained in the spin-nonpolarized computational scheme are fairly high.

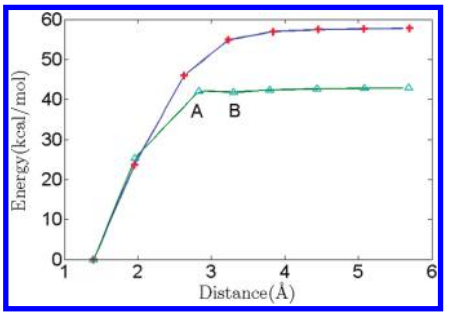

Figure 3. The axial N−NO_2 dissociation paths obtained from the spin nonpolarized ("crosses") DFT and spin polarized ("triangles") DFT computational schemes.

Not surprisingly, the situation changes when the spin polarized DFT method is used, indicating that the spin effects induced by nonpaired electrons are important for this reaction. Spin interactions, in fact, preclude the recombination of the split off nitro group with the rest of the HMX molecule for both axial and equatorial NO_2 groups. The corresponding formation energies in

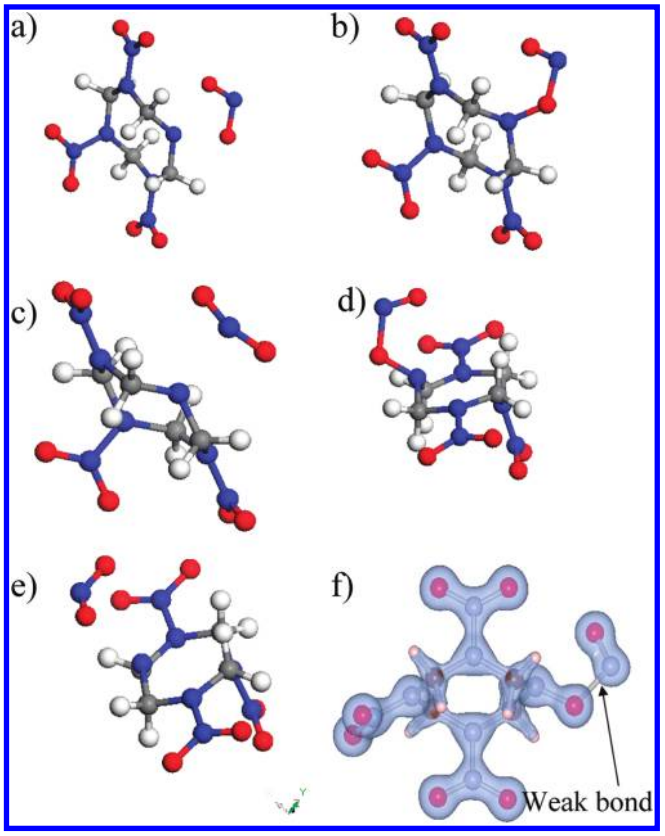

Figure 4. Illustration of how the calculations were organized, showing (a) how the NO_2 group was moved apart from the molecule and rotated to get to the state of interest (the final state for different mechanisms). Depending on the initial configuration, the system will go to the state (b or d), where (b) shows the nitro-to-nitrite isomerization in the "outward" NONO configuration with the corresponding transition state (c), and (d) shows the "inward" NONO configuration with the corresponding transition state (e). (f) The charge density plot for NONO shows the weak NO−NO bond.

the triplet states are 44.62 and 42.84 kcal/mol for the equatorial and axial groups, respectively. Figure 3, which displays the minimal energy path for the axial NO_2 as a function of the $N-NO_2$ distance, illustrates that the system stays in a singlet state up to the $N-NO_2$ distance of 2.83 Å, and favors the triplet state for larger separations. A careful examination of the energy profile reveals that there is a local minimum at 3.30 Å (B point in Figure 3) and the transition state at 2.83 Å (A point in Figure 3). This local minimum is very shallow, with the energy difference between A and B points (Figure 3) of only 0.3 kcal/mol; one can compare the value to k_BT at 1000 K that yields 2 kcal/mol. In other words, this finding means that the barrier for the reverse reaction is negligibly small and can be ignored.

Overall, the barrier heights of $N-NO_2$ fission reactions are comparable or slightly lower than the HONO formation activation energies for both the axial and equatorial nitro groups. In addition, the NO_2 moiety can recombine with the residue and restore the HMX molecule, unless it is engaged in other reactions right after the splitting, which would prevent the recombination.

Nitro-Nitrite Rearrangement. In investigations of the condensed phase decomposition, the observation has been made[50] that the deposed NO_2 fragment can recombine as a nitride, which can then decompose by breaking the O−N bond to form an NO, or attract hydrogen atoms and form a HONO (as described above) (see, for example, refs 14 and 20). In modeling the nitro-nitrite isomerization reaction as a precursor for the NO elimination, we introduce a rotation of NO_2 following the extension of the N−N bond, as shown in Figure 4a. During the relaxation, one of the O atoms binds with the N2 atom and forms a NONO isomer structure. Two different NONO configurations originating from the equatorial NO_2 were probed, with the "arm" faced outward (Figure 4b) and inward (Figure 4d). Only one axial NONO structure was simulated. Spin polarized DFT exhibits a difference only for the "inward" NONO. This reaction also has a low activation barrier at 44.39 kcal/mol and formation energy of 22.81 kcal/mol (Table 4). The system at the transition point is in the triplet state, while in the final configuration it favors the singlet state. We note that such a reaction accompanied by the spin change has a low probability in the gas phase because of quantum selection rules (this is a spin-forbidden transition). Therefore, we take this geometrical configuration at the transition point and recalculate its energy for the singlet state. In the obtained singlet state, forces remain zero and the total energy differs only by 0.1 eV from the triplet energy, as is observed in singlet−triplet crossing. Hence, the resulting configuration may be considered the transition state along the minimal energy path, and whether the system is allowed to go to triplet or it remains in singlet, the activation barriers are nearly the same. For two other reactions, the system prefers the singlet state and whether the spin polarized or nonpolarized DFT is used does not change the results. The reaction energies for two other reactions, "outward" equatorial NONO and axial NONO, are fairly similar (22.03 kcal/mol for the axial NONO and 22.89 kcal/mol for the equatorial NONO), whereas the activation barriers are relatively higher (49.84 kcal/mol for the "outward" equatorial isomer and 57.09 kcal/mol for the axial isomer) (Table 4). At the final configuration, the NO is only loosely bound to the molecule (Figure 4f), indicating that the NO will easily split off. This is also illustrated by the charge density plot in Figure 4f, which shows that the NO is virtually dissociated from the molecule. Observe that the O1−N1 bond (1.69 Å) is considerably longer and therefore weaker than the O1−N2 bond (1.37 Å). Thus, we established that the favorable nitro-nitrite isomerization reactions require overcoming the energy barrier, which is comparable to both the HONO elimination and the $N-NO_2$ fission reactions. This evaluation apparently concludes that, based on energetic considerations, all three mechanisms would be activated at nearly the same energy and they should be competing in the gas phase decomposition process of HMX.

Breaking the Ring. Further, although breaking the ring does not appear to us as a probable decomposition pathway in HMX, several researchers have suggested this possibility over the years, and therefore, we considered three additional dissociation mechanisms: a symmetric dissociation into two or four moieties and the formation of an open RDX structure. The early mass spectrometry study of thermal decomposition of HMX at T = 503, 527, and 553 K identified a concerted decomposition into four methylenenitramine $C_4H_8N_8O_8 \rightarrow 4CH_2N_2O_2$, which can further decompose into CH_2O and N_2O.[51] The observed major decomposition product with m/e = 148 led to a proposed homolytic cleavage of HMX into two $C_2H_4N_4O_4$ fragments that might further decompose to form methylenenitramine via $C_2H_4N_4O_4 \rightarrow 2CH_2N_2O_2$ (ref 52). Two competing global mechanisms for the thermal decomposition of HMX were also suggested,[53] the first leading to four HONO and HCN via

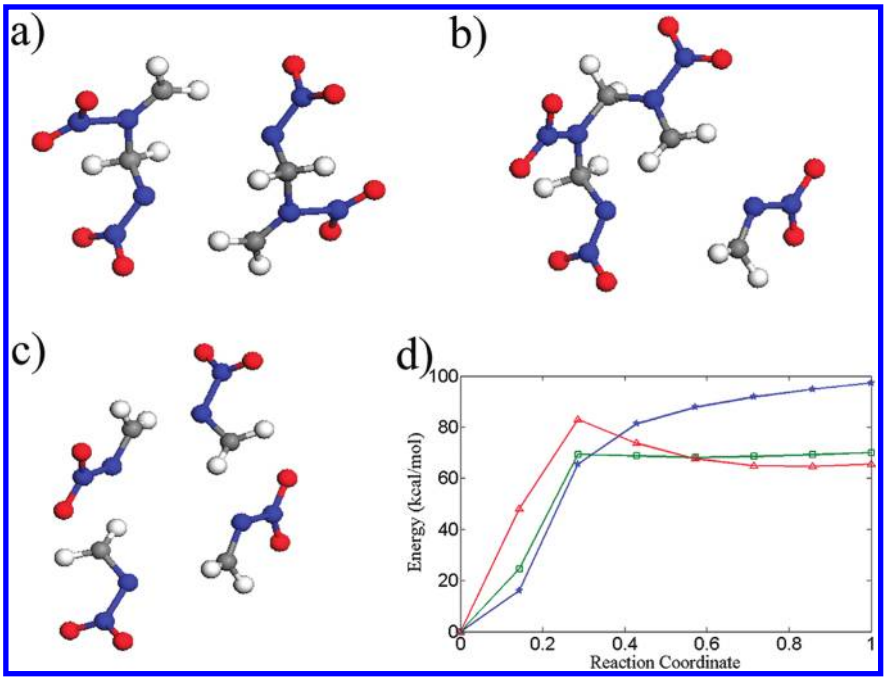

Figure 5. Simulated possible ways of breaking the molecular ring: (a) a symmetric two-way split of the ring, $C_4H_8N_8O_8 \rightarrow 2CH_4N_4O_4$, (b) an open RDX structure, $C_4H_8N_8O_8 \rightarrow CH_2N_2O_2 + C_3H_6N_6O_6$, (c) a fission of the ring into four parts, $C_4H_8N_8O_8 \rightarrow 4CH_2N_2O_2$, and (d) the corresponding minimal energy paths for these three reactions, two-way split of the ring (stars), open RDX structure (squares), and four-way split (triangles), respectively.

$C_4H_8N_8O_8 \rightarrow 4(HONO + HCN)$ or $C_4H_8N_8O_8 \rightarrow 4(NO_2 + HCN + H)$ and the second leading to the formation of four CH_2O and N_2O via $C_4H_8N_8O_8 \rightarrow 4(CH_2O + N_2O)$.

First, in simulating possible ways of breaking the ring, a symmetric split was probed by breaking C1−N2 and C3−N6 bonds (Figure 5a). After the relaxation, two parts of the molecule remained separated and did not recombine. The formation energy of two $C_2H_4N_4O_4$ moieties is 97.28 kcal/mol, which is significantly higher than the activation energy of other simulated reaction pathways. Second, by removing $CH_2N_2O_2$ from the HMX molecule configuration, we form an open ring RDX structure (Figure 5b).[54] After the relaxation, $CH_2N_2O_2$ remains stable and does not rebind to the ring, and the rest of the molecule retains its open RDX structure. The reaction energy is 69.96 kcal/mol. Third, fission of the ring by breaking the molecule into four equal $CH_2N_2O_2$ moieties[19,54] (Figure 5c) requires energy of 65.50 kcal/mol. In Figure 5d, we show results of the CNEBM calculations of minimal energy paths for all three reactions. Only the last reaction has a well-defined transition point; other pathways correspond to the barrier-less reactions. All three ways of possible breaking the molecular ring require fairly high activation barriers and are unlikely viable initiation mechanisms of the HMX decomposition in the gas phase.

III.2. Ideal Bulk HMX Crystal. Modeling decomposition reactions in the solid state is much more complex than the gas-phase processes. The smallest crystalline cell suitable for studying the decomposition reactions in crystalline β-HMX is found to be a $2 \times 2 \times 2$ supercell, which contains eight HMX molecules and a total of 448 atoms. The system simulated by a smaller unit cell collapses due to a large strain induced by unphysical strong interactions of the reactants in periodically translated supercells. In modeling solid-state chemistry, we follow our study of the gas phase (see section III.1) and limit the decomposition mechanisms to considering $N-NO_2$ homolysis and HONO and NONO isomerization reactions. There are two good reasons not to consider ring breaking reactions. First, the reactions exhibit high activation barriers and low reaction rates and hence are considered as unfavorable mechanisms even in the gas phase. The crystalline field will further suppress those mechanisms. Second, the reactions will require a significant activation volume, which is not available in the densely packed ideal HMX lattice.

In simulating the $N-NO_2$ cleavage, we observe once again that the equatorial and axial NO_2 isomers behave differently. First, we extended the N−N equatorial bond to probe several different distances and found that the system tends to restore the broken bond. Only a removal of the equatorial NO_2 far away from the parent molecule, for example, to another molecular layer in the crystal, enables it to find a stable position in the lattice. However, the energy required for such a process is very high, 74.33 kcal/mol, which makes us believe that the movement is unrealistic at least until fairly high temperature, and that breaking the equatorial bond is unfavorable. Next, a stable configuration of the axial nitro group is found at the N−N bond extension of 2.44 Å (Figure 6a). Unlike the corresponding molecular case, the barrier of the reverse reaction is not negligible, 1.78 kcal/mol (Figure 6b). The formation energy for the homolytically dissociated NO_2 is 46.09 kcal/mol, and the activation barrier is 47.87 kcal/mol. In the final configuration, the system favors the triplet state, and at the transition point, the singlet and triplet states have close total energies. Hence, the significant new feature brought by the crystalline environment of the decomposing HMX molecule is appreciable discrimination against the equatorial nitro group in favor of the axial nitro group.

Next, we consider the HONO elimination mechanisms. The calculated activation barriers for the hydrogen transfer to the equatorial and axial nitro groups are 52.27 and 47.93 kcal/mol,

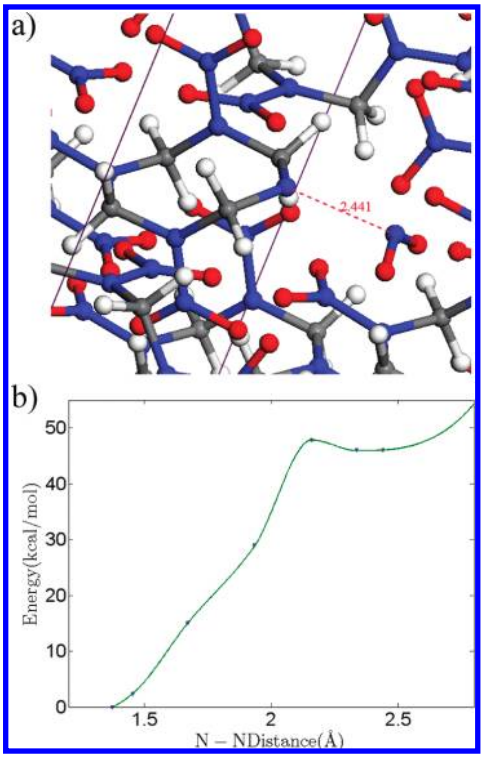

Figure 6. (a) Modeling of the N−NO_2 bond break in bulk HMX lattice. (b) The minimal energy path for N−NO_2 homolysis.

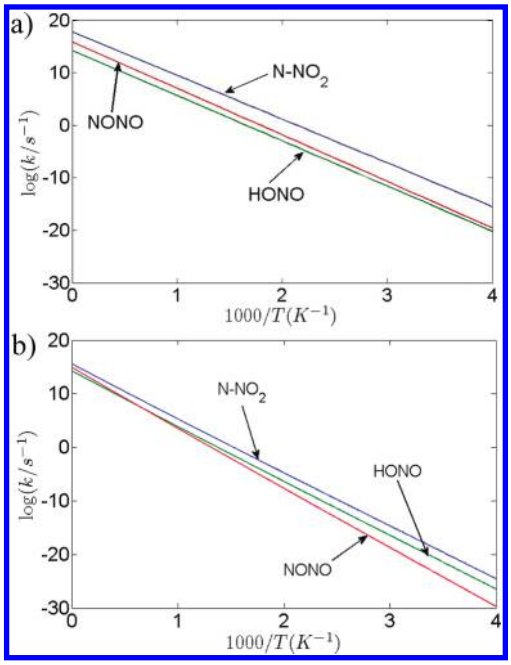

Figure 7. Reaction rates as a function of temperature for N−NO_2 homolysis, e-HONO elimination, and e-NONO isomerization reactions shown for the (a) gas phase and (b) crystalline phase.

respectively. From a comparison with the corresponding gas-phase decomposition barriers (44.62 and 42.84 kcal/mol, see Table 4), both the equatorial and axial groups exhibit higher activation energies in the crystalline environment than in a vacuum. However, the equatorial nitro group suffers the greater barrier increase than the axial nitro group, coherent with the N−NO_2 bond breaking scenario. This observation is also consistent with the crystalline arrangement of the system at the transition state. As mentioned earlier, the N−NO_2 distance at the transition point of the equatorial NO_2 is 0.5 Å larger than that of the axial nitro group. This implies that the equatorial HONO at the transition state is more influenced by surrounding molecules than the axial HONO isomer. Indeed, for the equatorial HONO, the N−N distance reduces by 0.17 Å as compared to the gas phase configuration, while, for the axial HONO, it reduces only by 0.03 Å. The results attest that the HONO elimination mechanism in the condensed phase also favors the axial nitro group to initiate the dissociation process over the equatorial group.

For the nitro-nitrite rearrangement (NONO) in the crystal, we also see some changes in the geometry configuration and activation energies. The activation barriers for the equatorial and axial reactions are 53.92 and 52.74 kcal/mol, to be compared to the corresponding energies in the gas phase, 44.39 and 57.09 kcal/mol. The equatorial NONO isomer at the transition point prefers the singlet state, while the singlet−triplet crossing occurs in the gas phase. Note that, for all reactions, the activation barriers are lower in the gas phase than in the solid phase. The only exception is the axial nitro-nitrite isomer, which has a higher activation barrier in the gas phase than that in the condensed phase. Contrary to expectations, the nitro-nitrite isomerization reaction does not preserve its intramolecular character and becomes a high energy reaction in the crystal while it was the probable competing decomposition mechanism in the gas phase.

Overall, in an ideal solid HMX, all three feasible dissociation pathways have higher activation barriers than in the gas phase. The lowest energy is required for the N−NO_2 cleavage, with visible preference given to the axial nitro group, while the equatorial group becomes more stable in the condensed phase than in the isolated molecule. The next is the intramolecular hydrogen transfer, leading to the HONO elimination, and the nitro-nitrite rearrangement, leading to NO−NO splitting, is the least favorable in the crystal, as it has a somewhat higher activation barrier than other dissociation mechanisms. We would like to reiterate that these conclusions are based on the energy balances alone. Now, we will include the ab initio kinetics in our consideration to complete the picture and validate (and refine) the obtained conclusions.

IV. REACTION RATES

We estimate reaction rates within the transition state theory.[55] For the HONO elimination and NONO rearrangement scenarios, the decomposition reactions have well-defined transition states. Therefore, the conventional TST is applicable to calculate the corresponding reaction rates. The N−NO_2 homolysis reaction proceeds with no barrier, and the variational transition state theory is employed to find the corresponding reaction rate. Given that quantum tunneling is ignored, the reaction rate within the conventional TST can be written as[31]

$$k = \frac{k_B T}{h} \frac{Z^{TS}}{Z^0} e^{-E_B/k_B T} \quad (2)$$

where Z^{TS} and Z^0 are partition functions at the transition and initial points, respectively, h is the Planck constant, k_B is the Boltzmann constant, T is the temperature, and E_B is the barrier height. Because the mass of an HMX molecule is appreciably

larger than those of NO_2, HONO, and NONO, we can assume that the HMX molecule is immobile. Therefore, we can ignore a rotation of the whole molecule and assume that only vibrations contribute to the partition function. The partition function due to vibrations can be calculated as

$$Z = \prod_{i-1}^{m} \frac{1}{2\sinh(\hbar\omega_i/k_B T)} \quad (3)$$

where w_i are vibrational frequencies, m is the number of vibrational modes, which for a molecule with N atoms is equal to $3N-6$ at the initial point and $3N-7$ at the transition point. We can separate zero point energy contributions of vibrations from the partition function and move them into the exponent. By doing so, we obtain

$$k = \frac{k_B T}{h} \frac{\prod_{i-1}^{3N-6}(1-e^{-\hbar\omega_i^0/k_B T})}{\prod_{i-1}^{3N-7}(1-e^{-\hbar\omega_i^{TS}/k_B T})} e^{-\bar{E}_B/k_B T} \quad (4)$$

Here, $\bar{E}_B$ is the zero point energy corrected barrier height.

$$\bar{E}_B = E_B - \frac{1}{2}\left(\sum_{i=1}^{3N-6}\hbar\omega_i^0 - \sum_{i=1}^{3N-7}\hbar\omega_i^{TS}\right) \quad (5)$$

Further, we calculate vibrational frequencies. A detailed study of the kinetics of the gas phase $N-NO_2$ homolysis reaction is reported elsewhere.[55] Briefly, one has to take into account the rotational motion of NO_2 around its axis and the motion of NO_2 around the HMX molecule. Since there is no well-defined transition point, the calculated reaction rate was obtained as a function of the $N-NO_2$ distance, and the minimum found was designated as the transition state. The zero point energy in this case reduces the barrier height to 38.1 kcal/mol. The obtained effective barrier heights for a-HONO and e-NONO are derived as 39.4 and 40.5 kcal/mol, respectively.

Note that, in the gas phase, all vibrational frequencies of the equilibrium HMX molecule and the molecule at the transition point are calculated. In the crystalline phase, this is a very computationally demanding task, since the HMX supercell has 1344 degrees of freedom. An attempt to include all possible vibrations in the calculation would make it forbiddingly expensive. Therefore, one way to limit required computational resources and make our calculations practical without losing the accuracy of the methodology is to choose only those vibrations that are critical for the process of interest and ignore others. Hence, we allow all vibrations of atoms in only one HMX molecule, which undergoes the dissociation, and fix all other atoms in the supercell. This way, we effectively represent our HMX molecule in the "frozen" crystalline field of the surrounding molecules and assume that changes in vibrational frequencies in all atoms from the surrounding are negligible. This approximation is well justified due to the nature of the molecular materials in which interactions among molecules are significantly weaker than intramolecular interactions. The obtained zero point energy corrected barriers of the chemical reactions are given in Table 4; the corrections range from 3 to 5 kcal/mol.

Parts a and b of Figure 7 depict the reaction rates as a function of $1/T$ for both the gas and solid phases. In the gas phase, the $N-NO_2$ homolysis is the dominant reaction because it progresses 2−5 orders of magnitude faster than NONO and HONO both of which have comparable rates. Recall that the activation barriers for all three mechanisms were fairly close (38.1, 39.4, and 40.5 kcal/mol, Table 4). In the solid phase, the $N-NO_2$ homolysis is also the fastest reaction. However, it is only an order of magnitude faster than the two other mechanisms. Therefore, one should conclude that, unlike the gas phase, all three reactions will significantly contribute in the decomposition of the crystalline HMX at high temperatures. At low temperatures, the $N-NO_2$ homolysis dominates, while a contribution from the NONO isomerization is visibly less important.

V. DISCUSSION AND CONCLUSIONS

An extensive theoretical and computational investigation of the initiation of chemical decomposition reactions in the gaseous and crystalline molecular material has been performed by means of combined density functional theory and transition state theory methods. The reaction energies, activation barriers, structures of transition states, and reaction rates were obtained and analyzed for a representative and extremely complex molecular material β-HMX, which has been and is being extensively studied, and yet is poorly understood. In the gas phase, several possible primary reaction steps were simulated, including the direct $N-NO_2$ bond homolysis, the intramolecular hydrogen transfer (HONO elimination), the nitro-nitrite rearrangement (NONO-isomer formation leading to NO elimination), and the concerted ring fissions into four or two symmetric moieties and a single C−N bond cleavage leading to the formation of an open RDX structure. On the basis of the revealed energetic trends and estimated reaction rates, only low energy reactions, $N-NO_2$ fission, HONO, and NONO isomerizations, were simulated in the solid phase.

It was established that the lowest energy decomposition reaction in the gas phase is the $N-NO_2$ homolysis, which requires overcoming a barrier of 42.8 kcal/mol for the axial nitro group and 44.6 kcal/mol for the equatorial nitro group (Table 4). The calculated energies are in excellent agreement with the earlier B3LYP density functional theory study with the 6-31G(d) basis set, which reported the barrier of 44.6 kcal/mol (ref 21) and 46.7 kcal/mol, obtained with a larger basis set, 6-311++G-(3df,3pd),[56] as well as with calculations of the relevant molecule, dimethylnitramine, 46.8 kcal/mol (ref 7) and 44.7 kcal/mol (ref 30). Once vibrational frequencies are taken into account, the activation barriers are reduced by about 5 kcal/mol and yield 38−40 kcal/mol. Further, the barriers of the HONO elimination and NONO isomer formation are found to be only a few kcal/mol higher, 43.39 and 44.39 kcal/mol for the axial HONO and the equatorial NONO, respectively. However, we also found that, despite the small differences in the activation energies of all three decomposition mechanisms, the performed transition state theory calculations show that the $N-NO_2$ fission proceeds with a rate that is 2−5 orders of magnitude higher than the other two reactions. We suggest that this is mostly due to the vibrations of the $N-NO_2$ critical bond and the relative motion of the nitro group with respect to the rest of the molecule that make large contributions to the partition function.[55] The obtained barriers (38−41 kcal/mol) fall into the range 32−53 kcal/mol reported based on the thermal gas-phase decomposition measurements and thermochemical estimates.[6,12,26,29] On one hand, the closeness of the calculated barriers for all three reactions explains the observed nitrogen oxides and water among the products in the mass spectroscopy experiments. On the other hand, the kinetics and concentrations of observed decomposition products in global thermal decomposition experiments[6,9−12] can be accurately

interpreted with the derived reaction rates: while all three dissociation reactions are activated at almost the same energy, the N−NO_2 homolysis prevails in comparison to the two other mechanisms.

In the solid-state decomposition, a *perfect* crystalline HMX[18] still favors the N−NO_2 fission with the activation barrier of the axial nitro group at 47.87 kcal/mol (43.67 kcal/mol, once the zero point energy correction is included). It nearly coincides with the axial HONO elimination barrier of 47.93 kcal/mol (45.01, with the zero point energy correction). This is consistent with the finding obtained by ReaxFF molecular dynamics that suggested that the initial steps of HMX decomposition in the condensed phase involve homolytic cleavage of the N−NO_2 bond, with formation of NO_2 and, to a lesser extent, HONO.[57] The nitro-nitrite isomerization pathway has the highest barrier at 52.7 kcal/mol (49.22, with the zero point energy correction). All three reaction barriers are within the experimentally reported range of 13−67 kcal/mol.[27] The wide range of values is expected in solid phase reactions. The factors that control the degradation of materials, for example, solid−solid phase transitions, pressure, autocatalysis, and others, have less influence on the gas phases. The solid state calculations reveal that the crystalline field, or interactions among molecules, affects the decomposition process in several ways. All three activation barriers are higher in the solid than in the isolated HMX molecule, with the N−NO_2 break and HONO formation being almost the same and the NONO isomerization becoming the least favorable. The equatorial nitro group is much more stable than the axial nitro group, implying that the dissociation will start with breaking the axial N−N bonds. The N−NO_2 homolysis has a well-defined transition state, though the relevant minimum of the potential energy profile is very shallow. The N−NO_2 fission, while having the highest rate similarly to the gas phase process, progresses appreciably slower in the solid phase than in the gas phase. In contrast, rates of the HONO elimination and the NONO isomer formation in bulk do not differ much from gas. Most importantly, neglect of the kinetics leads to the erroneous conclusion. For example, in the gas phase HMX, all three decomposition mechanisms appear almost equally probable, which contradicts experimental observations. This is immediately corrected once the reaction rates are considered, as they prove that the N−NO_2 is the most efficient decomposition mechanism and the other two contribute very little. As to the solid HMX, the N−NO_2 and HONO elimination have similar activation energies, while the NONO mechanism, in fact, is visibly faster than the HONO elimination. The overall conclusion is that at low temperatures the N−NO_2 homolysis dominates the condensed phase decomposition, while at high temperatures all three mechanisms contribute to the process of the material degradation.

The comparison of the calculated reaction rates predicts that gas phase HMX decomposes faster and requires lower activation energies than the solid. While the latter is in harmony with experiments, the former is in contrast with available data (see, for example, refs 6 and 12). Generally, condensed high explosives exhibit higher sensitivity to external stimuli and decompose faster than gas phase materials. We speculate that our study falls short in catching this effect because the presence of defects and deformations was neglected. There is convincing evidence that certain imperfections and charged or excited states affect chemical reactions in energetic materials[58] and have to be taken into account to make reliable predictions about material properties.

Most notably, this study demonstrates that calculations of the decomposition reactions of extremely complex molecular materials are theoretically challenging and computationally demanding, yet modern tools are making those calculations possible and even practical at this time. The lack of experimental chemical kinetic rate constant data currently prohibits building more complex reaction schemes.[8] Only a few modern experiments are currently yielding reaction product formation data.[8] Ab initio calculations can provide sufficient data and analysis to disaggregate global kinetics measurements and to interpret experiments unambiguously.[59] The strategies similar to those presented in this illustrative study can be applied to other molecular, supramolecular, and hierarchical materials and systems to enable reliable predictions and possible tuning of their properties as well as design of new materials with targeted functionalities.

■ ACKNOWLEDGMENT

This work is supported in part by ONR Grant No. N00014-09-1-0225 and by NSF Grant No. DMR-100054. This research used resources of the NERSC, which is supported in part by the U.S. DOE under Contract No. DE-AC02-05CH11231. M.M.K. is grateful to the Office of the Director of National Science Foundation for support under the Independent Research and Development Program. Any appearance of findings, conclusions, or recommendations expressed in this material are those of the authors and do not necessarily reflect the views of NSF.

■ REFERENCES

(1) Also known as cyclotetramethylene-tetranitramine, tetrahexamine tetranitramine, or octahydro 1,3,5,7-tetranitro-1,3,5,7-tetrazocane, HMX was first made in 1930. HMX is widely used in military applications, including as the detonator in nuclear weapons, in the form of polymer-bonded explosive, and as a solid rocket propellant. Recently, it also found applications in shock synthesis of super hard and super dense materials; see, for example, synthesis of nano-diamond: Kozyrev, N. V.; Larionov, B. V.; Sakovich, G. V. *Combust., Explos. Shock Waves* **2008**, *44*, 193–197.

(2) Fedoroff, B. T.; Sheffield, O. E. *Encyclopedia of Explosives and Related Items*; Picatinny Arsenal: Dover, NJ, 1966; pp F217−F223.

(3) Farber, M.; Srivastava, R. D. Proc. 16th JANNA Combust. Meeting 1979, CPIA pub. 308, p 59.

(4) Vandersall, K. S.; Tarver, C. M.; Garcia, F.; Chidester, S. K. *J. Appl. Phys.* **2010**, *107*, 094906–094906-11.

(5) Yoh, J. J.; McClelland, M. A.; Maienschein, J. L.; Nichols, A. L.; Tarver, C. M. *J. Appl. Phys.* **2006**, *100*, 073515–073515-9.

(6) Brill, T. B.; James, K. J. *Chem. Rev.* **1993**, *93*, 2667–2692.

(7) Melius, C. F.; Piqueras, M. C. *Proc. Combust. Inst.* **2002**, *29*, 2863–2871.

(8) Tarver, C. M.; Tran, T. D. *Combust. Flame* **2004**, *137*, 50–62.

(9) Behrens, R.; Bulusu, S. *J. Phys. Chem.* **1991**, *95*, 5838–5845.

(10) Behrens, R.; Bulusu, S. *J. Phys. Chem.* **1992**, *96*, 8877–8891.

(11) Brill, T. B.; Brush, P. J. *Philos. Trans. R. Soc., A* **1992**, *339*, 377–385.

(12) Brill, T. B.; Beckstead, M. C.; Flanagan, J. E.; Lin, M. C.; Litzinger, T. A.; Waesche, R. H. W.; Wight, C. A. Chemical Speciation and Dynamics in the Surface Combustion Zone of Energetic Materials, review. *J. Propul. Power* **2002**, *18*, 824–834.

(13) Miller, M. S. *Combust. Flame* **1982**, *46*, 51–73.

(14) Melius, C. F. *J. Phys. (Paris)* **1987**, *48*, C4–341−352.

(15) Cobbledick, R. E.; Small, R. W. H. *Acta Crystallogr., Sect. B* **1974**, *30*, 1918–1922.

(16) Henson, B. F.; Smilowitz, L.; Asay, B. W.; Dickson, P. M. *J. Chem. Phys.* **2002**, *117*, 3780–3788. Smilowitz, L.; Henson, B.; Asay, B.; Dickson, P. *J. Chem. Phys.* **2002**, *117*, 3789–3798.

(17) Smilowitz, L.; Henson, B. F.; Greenfield, M.; Sas, A.; Asay, B. W.; Dickson, P. M. *J. Chem. Phys.* **2004**, *121*, 5550–5552.
(18) Note that an effect of $\beta \rightarrow \delta$ phase transition on decomposition of HMX is neglected in this study. A mechanism for $\beta \rightarrow \delta$ phase transition was found to be greatly affected by the presence of a nitroplasticizer (the eutectic mixture of bis(2,2-dinitropropyl)acetal and bis(2,2-dinitropropyl)formal) in the HMX based formulation, by particle size, and by temperature. See ref 17 for details. In our present article, we focus on chemical reactions in ideal HMX crystals, in the absence of binders, internal surfaces and voids, or other imperfections. The fact that the phase transition occurs just before or during the onset of thermal decomposition, as discussed in ref 8, emphasizes the importance of careful studies of decomposition from both phases, β and δ, in addition to modeling the phase transition explicitly. Because the β-phase of HMX is the most stable crystalline phase at room temperature, it appears most reasonable to start studying the decomposition from this phase. Similar calculations can be performed for other phases and various external conditions.
(19) Lewis, J. P. *Chem. Phys. Lett.* **2003**, *371*, 588–593.
(20) Manaa, M. R.; Fried, L. E.; Melius, C. F.; Elstner, M.; Frauenheim, Th. *J. Phys. Chem. A* **2002**, *106*, 9024–9029.
(21) Chakraborty, D.; Muller, R. P.; Dasgupta, S.; Goddard, W. A. *J. Phys. Chem. A* **2001**, *105*, 1302–1314.
(22) Lewis, J. P.; Glaesemann, K. R.; VanOpdorp, K.; Voth, G. A. *J. Phys. Chem. A* **2000**, *104*, 11384–11389.
(23) Flournoy, J. M. *J. Chem. Phys.* **1962**, *36*, 1107–1108.
(24) Korsunskii, L.; Dubovitskii, F. I. *Dokl. Akad. Nauk SSSR* **1964**, *155*, 402–410. *Russ. Chem. Rev.* **1981**, *50*, 958–978.
(25) Lazarou, Y. G.; Papagiannakopoulos, P. *J. Phys. Chem.* **1990**, *94*, 7114–7119.
(26) Oxley, J. C.; Kooh, A. B.; Szekeres, R.; Zheng, W. *J. Phys. Chem.* **1994**, *98*, 7004–7008.
(27) Brill, T. B.; Arisawa, H.; Brush, P. J.; Gongwer, P. E.; Williams, G. K. *J. Phys. Chem.* **1995**, *99*, 1384–1392.
(28) Nigenda, S. E.; McMillen, D. F.; Golden, D. M. *J. Phys. Chem.* **1989**, *93*, 1124–1130.
(29) Brill, T. B.; Gongwer, P. E; Williams, G. K. *J. Phys. Chem.* **1994**, *98*, 12242–12247.
(30) Velardez, G. F.; Alavi, S; Thompson, D. L. *J. Chem. Phys.* **2005**, *123*, 074313–074313−8.
(31) Hanggi, P; Talkner, P; Borkovec, M. *Rev. Mod. Phys.* **1990**, *62*, 251–341.
(32) Garrett, B. C.; Truhlar, D. G. *J. Phys. Chem.* **1979**, *83*, 1052–1079.
(33) The effect of defects, surfaces and voids, and shear-strain deformations on the stability of HMX will be reported in detail elsewhere. For preliminary results and discussion, see: Sharia, O.; Kuklja, M. M. Effect of defects on initiation of chemistry in HMX. In *Shock Compression of Condensed Matter - 2009*; Elert, M. L., Buttler, W. T., Furnish, M. D., Anderson, W. W., Proud, W. G., Eds.; AIP conference proceedings 1195; American Institute of Physics: Melville, NY, 2009; pp 353−356.
(34) Hohenberg, P.; Kohn, W. *Phys. Rev.* **1964**, *136*, B864–B871.
(35) Kohn, W.; Sham, L. J. *Phys. Rev. A* **1965**, *140*, A1133–A1138.
(36) Perdew, J. P.; Burke, K.; Ernzerhof, M. *Phys. Rev. Lett.* **1996**, *77*, 3865–3868.
(37) Blöchl, P. E. *Phys. Rev. B* **1994**, *50*, 17953–17979.
(38) Kresese, G.; Furthmuller, J. *Comput. Mater. Sci.* **1996**, *6*, 15–50.
(39) Kresse, G.; Furthmuller, J. *Phys. Rev. B* **1996**, *54*, 11169–11186.
(40) Kresse, G.; Hafner, J. *Phys. Rev. B* **1993**, *47*, 558–561.
(41) Monkhorst, H. J.; Pack, J. D. *Phys. Rev. B* **1976**, *13*, 5188–5192.
(42) Cady, H. H .; Larson, A. C.; Cromer, D. T. *Acta Crystallogr.* **1963**, *16*, 617–623.
(43) Choi, C. S.; Boutin, H. P. *Acta Crystallogr.* **1970**, *B26*, 1235–1240.
(44) Zerilli, F.; Kuklja, M. *J. Phys. Chem. A* **2006**, *110*, 5173–5179. Zerilli, F.; Kuklja, M. *J. Phys. Chem. A* **2010**, *114*, 5372–5376.
(45) Henkelman, G.; Uberuaga, B. P.; Jonsson, H. *J. Chem. Phys.* **2000**, *113*, 9901–9904.
(46) Eyring, H. *Chem. Rev.* **1935**, *17*, 65–77.
(47) Similar calculations can be preformed to take into account pressure and shear-strain effects.
(48) We focus in this work on an intramolecular hydrogen transfer only and do not consider an intermolecular transfer between adjacent molecules, as the major important goal of this work is a comparison of the gas-phase and solid-state decomposition mechanisms. Modeling of the intermolecular transfer based on simulations of two isolated molecules proved to be unreliable and may lead to erroneous conclusions. See, for example, the discussion in: Kimmel, A. V.; Sushko, P. V.; Shluger, A. L.; Kuklja, M. M. *J. Phys. Chem. A* **2008**, *112*, 4496–4500.
(49) It is reasonable to suggest that the decomposed HMX molecule will be in a triplet state, when the split off NO_2 group is moved far away; however, most of the time it is impossible to know what state is energetically preferred, singlet or triplet. Therefore, without making any *a priori* assumptions about the spin state of the system, we used both the spin polarized and spin nonpolarized computational schemes to explore how the total spin of the system affects the decomposition process.
(50) Melius, C. F. In *Chemistry and Physics of Energetic Materials*; Bulusu, D. N., Ed.; Kluwer: Dordrecht, The Netherlands, 1990.
(51) Suryanarayana, B.; Graybush, R. J.; Autera, J. R. *Chem. Ind. (London, U. K.)* **1967**, *52*, 2177–2179.
(52) Farber, M. Srivastava, R. D. Proc. 16th JANNA Combust. Meeting 1979, CPIA pub. 308, p 59.
(53) Brill, T. B. J. *Prop. Power* **1995**, *11*, 740–751.
(54) Shaw, R.; Walker, F. E. *J. Phys. Chem.* **1977**, *81*, 2572–2576.
(55) For more details regarding HMX gas phase kinetics calculations, see: Sharia, O.; Kuklja, M. M. *J. Phys. Chem. A* **2010**, *114*, 12656–12661.
(56) Cobos, C. J. *THEOCHEM* **2005**, *714*, 147–152.
(57) Zhang, L. Z.; Zybin, S. V.; van Duin, A. C. T.; Dasgupta, S.; Goddard, W. A., III. *J. Phys. Chem. A* **2009**, *113*, 10619–10640.
(58) Kuklja, M. M. *J. Phys. Chem. B* **2001**, *105*, 10159–10162. Kuklja, M. M.; Stefanovich, E. V.; Kunz, A. B. *J. Chem. Phys.* **2000**, *112*, 3417–3423. Kuklja, M. M.; Rashkeev, S. N. *J. Chem. Phys. C* **2009**, *113*, 17–20. Kuklja, M. M.; Rashkeev, M. M. *Phys. Rev. B* **2007**, *75*, 104111–104111-10. Kuklja, M. M.; Rashkeev, S. N. *Appl. Phys. Lett.* **2007**, *90*, 151913–151916. Kuklja, M. M.; Rashkeev, S. N. *J. Phys. Chem. Lett.* **2010**, *1*, 363–367. Kuklja, M. M. *Appl. Phys. A: Mater. Sci. Process.* **2003**, *76*, 359–366.
(59) For alternative approaches, see, for example, research based on molecular dynamics: Isayev, O.; Gorb, L.; Qasim, M.; Leszczynski, J. *J. Phys. Chem. B* **2008**, *112*, 11005–11013; research based on hybrid QM/MM:Kimmel, V.; Munoz, R. D.; Sushko, P. V.; Shluger, A. L.; Kuklja, M. M. *Phys. Rev. B* **2009**, *80*, 134108–134108-12 (and ref 48).